J. Fluid Mech. (2010), *vol.* 662, *pp.* 514–539.
doi:10.1017/S0022112010003381

Universal aspects of small-scale motions in turbulence

G. E. ELSINGA[1,2]† AND I. MARUSIC[1]

[1]Department of Mechanical Engineering, The University of Melbourne, Melbourne, VIC 3010, Australia

[2]Laboratory for Aero and Hydrodynamics, Delft University of Technology, Leeghwaterstraat 21, 2628 CA, Delft, The Netherlands

(Received 30 September 2009; revised 15 June 2010; accepted 18 June 2010; first published online 22 September 2010)

Two aspects of small-scale turbulence are currently regarded universal, as they have been reported for a wide variety of turbulent flows. Firstly, the vorticity vector has been found to display a preferential alignment with the eigenvector corresponding to the intermediate eigenvalue of the strain rate tensor; and secondly, the joint probability density function (p.d.f.) of the second and third invariant of the velocity gradient tensor, Q and R, has a characteristic teardrop shape. This paper provides an explanation for these universal aspects in terms of a spatial organization of coherent structures, which is based on an evaluation of the average flow pattern in the local coordinate system defined by the eigenvectors of the strain rate tensor. The approach contrasts with previous investigations, which have relied on assumed model flows. The present average flow patterns have been calculated for existing experimental (particle image velocimetry) or numerical (direct numerical simulation) datasets of a turbulent boundary layer (TBL), a turbulent channel flow and for homogeneous isotropic turbulence. All results show a shear-layer structure consisting of aligned vortical motions, separating two larger-scale regions of relatively uniform flow. Because the directions of maximum and minimum strain in a shear layer are in the plane normal to the vorticity vector, this vector aligns with the remaining strain direction, i.e. the intermediate eigenvector of the strain rate tensor. Further, the QR joint p.d.f. for these average flow patterns reveals a shape reminiscent of the teardrop, as seen in many turbulent flows. The above-mentioned organization of the small-scale motions is not only found in the average patterns, but is also frequently observed in the instantaneous velocity fields of the different turbulent flows. It may, therefore, be considered relevant and universal.

Key words: isotropic turbulence, turbulent boundary layers, turbulent flows

1. Introduction

In this paper, we present average flow patterns in local coordinate systems, such as those defined by the eigenvectors of the strain rate tensor. The purpose is to identify the flow pattern (or coherent structures) responsible for some apparently universal aspects of small-scale turbulence, which are associated with local frames of reference (Tsinober 2001). These aspects are (i) the preferred alignment of the vorticity vector with the intermediate eigenvector of the strain rate tensor and (ii) the teardrop shape

† Email address for correspondence: g.e.elsinga@tudelft.nl

of the joint probability density function (p.d.f.) of the second and third invariant of the velocity gradient tensor, Q and R (Chong, Perry & Cantwell 1990). Moreover, the presented average patterns help clarify universal aspects of the organization of small-scale motions in turbulence and their relation to the larger energy-containing scales of motion.

1.1. *Background*

The orientation of the vorticity vector $\boldsymbol{\omega}$ relative to the eigenvectors of the rate of strain tensor $\boldsymbol{S}$ has received important attention in turbulent flows because of its relevance to the vorticity stretching term (i.e. $\boldsymbol{\omega}^T\boldsymbol{S}\boldsymbol{\omega}$) in the enstrophy equation. Results from both numerical simulations and experiments have indicated that $\boldsymbol{\omega}$ preferably aligns itself with the eigenvector corresponding to the intermediate eigenvalue of $\boldsymbol{S}$ (which will be referred to as the intermediate eigenvector in this paper). This behaviour has been observed in a broad range of turbulent flows as well as across Reynolds numbers (see e.g. Ashurst *et al.* 1987; Tsinober Kit & Dracos 1992; Vincent & Meneguzzi 1994; Kholmyansky, Tsinober & Yorish 2001; Lüthi, Tsinober & Kinzelbach 2005; amongst many others). These flows include isotropic turbulence, turbulent shear flow, turbulent boundary layers (TBLs) and atmospheric turbulence.

The alignment with the intermediate strain rate direction has been used to explain the limited growth rates observed for vorticity. Whereas vorticity prefers alignment with the intermediate eigenvector, material lines and passive vectors, which are measures for the mixing properties of turbulence, generally tend to be directed towards the direction of maximum strain and consequently experience greater average growth rates (Huang 1996; Ohkitani 2002; Lüthi *et al.* 2005).

Previous, geometric/kinematic explanations for the observed vorticity alignment relied on idealized flow patterns, i.e. the Burgers vortex and layer (Andreotti 1997), or assumed two-dimensional (2D) coherent vortex structures (Jimenez 1992). These arguments, however, contain some uncertainties in that the vortices are rarely 2D, and that the relation between the idealized flow and the full complexity of real turbulence is not obvious. Furthermore, some details remain to be explained, in particular for the core region of (quasi) 2D vortices, because vorticity aligns with the most stretching eigenvector, and *not* the intermediate eigenvector, in a finite region around the axis of a Burgers vortex (Andreotti 1997). The swirling motion in this region is nearly rotationally symmetric and consequently the strain rate tensor in this flow has two eigenvalues (i.e. principal strain rates) of equal sign and nearly equal in magnitude, which correspond to the eigenvectors in the plane of the swirling motion, and one eigenvalue related to the eigenvector in the direction of the swirling axis. Due to continuity requiring that the sum of the eigenvalues equals zero, the latter eigenvalue is of opposite sign to that of the other two, and consequently the swirling axis aligns with either the most compressing or the most stretching eigenvector, and not the intermediate eigenvector. In contrast, in turbulent flow the tendency for alignment with the intermediate eigenvector is observed to be stronger for increasing vorticity magnitude (e.g. Huang 1996), which is often concentrated in the core of (vortex) tubes (She, Jackson & Orszag 1990; Jimenez *et al.* 1993).

Alternatively, some explanations for the vorticity alignment with the intermediate eigenvector have been offered based on an analysis of the flow governing equations without considering the coherent structure explicitly. Ashurst *et al.* (1987) proposed that the alignment is a consequence of angular momentum conservation in a restricted Euler model of the flow ignoring viscosity and pressure interactions between turbulent eddies (Vieillefosse 1984; Cantwell 1992). Along similar lines, it has been shown,

assuming nonlinear and viscous terms in the vorticity equation are small, that strong straining of weak vorticity tends to produce sheets possessing the mentioned alignment (Kevlahan & Hunt 1997). Both mathematical models may explain the initial stages of the alignment of weak vorticity, but are not sufficient for intense vorticity at small scales where viscosity is deemed important. Furthermore, comparisons of the dynamic evolution of vorticity and passive material lines with and without diffusion (Ohkitani 2002; Lüthi *et al.* 2005) have indicated the importance of viscosity in maintaining the alignment of vorticity with the intermediate eigenvector and the vorticity dynamics in general. Nevertheless, the alignment has been observed in a vorticity sheet in real turbulence before the sheet rolled up into a vortex tube (Vincent & Meneguzzi 1994). The concentration of vorticity in sheets has also been observed by Passot *et al.* (1995), who additionally demonstrated by numerical simulation of individual sheets that under certain conditions multiple vortex tubes can result. Similar sequences of events have also been found to play an important role in the development of turbulence from initially random vorticity fields in direct numerical simulation (DNS) (Kida & Tanaka 1994; Horiuti & Fujisawa 2008). In a recent study, Goto (2008) ascribes the formation of small-scale vortices (i.e. energy cascade) directly to the straining by (counter-rotation) large-scale vortices. The fact that shear-layer roll-up was rarely observed could be due to this process being very fast as noted by the author. In any case, shear-layer roll-up is mainly a *dynamical* relation between sheets and vortices. Instantaneously, visualizations by Vincent & Meneguzzi (1994) revealed alignment of some vortices and Jimenez *et al.* (1993) presented some indication of background vorticity concentrated in sheets with tubes/worms embedded in this background. The relevance of sheets in various turbulent flows deserves further statistical investigation, such as proposed here, especially in the light of the mentioned kinematic models for the vorticity alignment in vortical structures.

The second potentially universal aspect of small-scale turbulent motion relates to the invariants of the velocity gradient tensor $\boldsymbol{A} = \nabla V$, which are $P = -A_{ii}$, $Q = -(1/2)A_{ij}A_{ji}$ and $R = -(1/3)A_{ij}A_{jk}A_{ki}$. These invariants completely define the generalized local flow topology with respect to the reference frame determined by the eigenvectors of $\boldsymbol{A}$, as outlined in Chong *et al.* (1990). Here, the term 'local' refers to a pointwise evaluation of the velocity gradient tensor. Note that for incompressible flow $P = 0$ due to continuity, so that the topology can be characterized using only Q and R. Joint p.d.f.s of Q and R across a variety of turbulent flows such as mixing layers, isotropic and wall-bounded turbulence have all revealed a self-similar teardrop shape (Soria *et al.* 1994; Blackburn, Mansour & Cantwell 1996; Chong *et al.* 1998; Ooi *et al.* 1999; Elsinga & Marusic 2010). And there is also some evidence to suggest that the similarity may even extend to compressible flows (Tsinober 2001). Although the teardrop appears from models for the pointwise velocity gradient evolution (Cantwell 1993; Biferale *et al.* 2007), the authors are not aware of a suitable comprehensive interpretation or explanation of this shape in relation to the small-scale coherent structures. Thus far these topics, though closely related, appear to have developed mostly separately. However, some observations concerning the invariants and physical quantities or coherent structures stand out. The points in the QR plane corresponding to a positive value of the discriminant $D = (27/4)R^2 + Q^3$ correspond mainly to (vortex) tube structures (Chong *et al.* 1998; Chacin & Cantwell 2000) and dissipation occurs mostly in the tail of the tear shape ($Q < 0$, $R > 0$) in points located near the tube structures in physical space (Chacin & Cantwell 2000). This spatial relation was also noted in a number of other studies (e.g. Kerr 1985; Ruetsch & Maxey 1991; Vincent & Meneguzzi 1994). These are partial observations, meaning

that specific physical quantities are put in relation to specific parts of the QR space. Hence no integral picture of the small-scale turbulent motions emerges directly from them.

1.2. *Methodology*

As mentioned above, the vorticity alignment and the invariants of the velocity gradient tensor $\boldsymbol{A}$ are evaluated in a local frame of reference defined by the local velocity gradients. Specifically, the orientation of the vorticity vector is determined relative to the eigenvectors of the strain rate tensor $\boldsymbol{S} = (\boldsymbol{A}^T + \boldsymbol{A})/2$. We therefore turn to the average flow patterns in this eigenframe to establish the statistically relevant flow structure responsible for these two aspects of small-scale turbulence. Furthermore, a statistical approach allows a direct comparison of different flows. In particular, we will consider here a TBL, a channel flow and homogeneous isotropic turbulence. As will be shown, these average patterns reveal a particular spatial arrangement of vortices and vorticity sheets, which is similar in appearance for all three turbulent flows, yet is strikingly different from that returned by a random divergence-free velocity field. Moreover, these average flow patterns can explain the observed teardrop shape of the invariants' joint p.d.f. It will, furthermore, be shown that this average pattern occurs frequently in the instantaneous flows. Based on these results the previously proposed kinematic explanations for the vorticity alignment can be refined and a comprehensive model can be constructed, which combines many of the small-scale turbulence features found in the literature. In this paper, the focus is on the flow kinematics leaving dynamical aspects for future work.

The turbulence datasets used in the present study originate from different sources. The boundary-layer data are from Schröder *et al.* (2008), who measured the full three-dimensional (3D) velocity distribution in water by tomographic particle image velocimetry (PIV) (Elsinga *et al.* 2006). The measurement volume covered the outer layer between 0.11δ and 0.30δ distance from the wall, where δ is the boundary-layer thickness. The Reynolds numbers based on momentum thickness and wall shear stress are $Re_\theta = 2460$ and $Re_\tau = 800$, respectively. The spatial resolution is 0.07δ equivalent to 56 wall units. The turbulent channel flow is DNS data from del Alamo *et al.* (2004). For this flow the Reynolds number based on skin friction is $Re_\tau = 934$. Compared to the experiment, the spatial resolution is higher for the channel DNS at approximately seven wall units in the outer region. Finally, the velocity distribution in forced homogenous isotropic turbulence at $Re_\lambda = 170$ has been provided by Dr A. A. Wray (CTR 2002, private communication). These data are from a DNS on a 256^3 grid using a classical pseudospectral code (e.g. Jimenez *et al.* 1993). The spatial resolution is this case is $k_{max}\eta = 1.25$, where k_{max} is the maximum resolved wavenumber and η is the Kolmogorov length scale.

The volumetric data allow an evaluation of all nine elements of the velocity gradient tensor $\boldsymbol{A}$. The strain rate tensor $\boldsymbol{S}$ is then given by the symmetric part of the velocity gradient tensor: $\boldsymbol{S} = (\boldsymbol{A}^T + \boldsymbol{A})/2$. The eigenvalues of $\boldsymbol{S}$, also referred to as the principal strain rates, will be denoted as σ_i and the corresponding eigenvectors as $\boldsymbol{\lambda}_i$. We will order the eigenvalues as $\sigma_1 > \sigma_2 > \sigma_3$. From incompressibility it follows that the sum of σ_i is zero, hence $\sigma_1 > 0$ and $\sigma_3 < 0$. The intermediate eigenvalue σ_2 can be positive or negative, but is reported to be positive on average (e.g. Betchov 1956; Ashurst *et al.* 1987). The orientation of the vorticity vector $\boldsymbol{\omega}$ within the coordinate system defined by the eigenvectors $\boldsymbol{\lambda}_i$ is commonly expressed by three angles $\theta_{\omega,i}$, which are determined from the inner products $\cos(\theta_{\omega,i}) = (\boldsymbol{\omega} \cdot \boldsymbol{\lambda}_i)/(|\boldsymbol{\omega}||\boldsymbol{\lambda}_i|)$. The p.d.f.s for these angles in the present boundary-layer dataset are shown in figure 1. In agreement with the literature

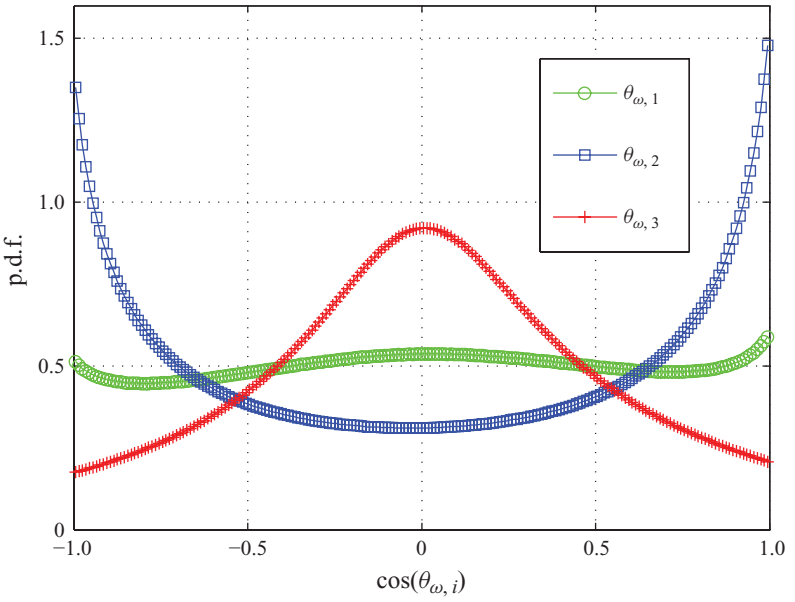

FIGURE 1. (Colour online) Probability density functions of the cosine of the angle between the vorticity vector and the three eigendirections of the strain rate tensor. The results are for the TBL.

the vorticity displays a preferential alignment with the intermediate eigenvector showing as an increased probability of $|\cos(\theta_{\omega,2})| = 1$. Furthermore, it is mostly oriented normal to the most compressing eigendirection $\boldsymbol{\lambda}_3$. The p.d.f. of the angle with eigenvector corresponding to the largest stretching $\boldsymbol{\lambda}_1$ is essentially flat, as expected.

In the following section, some basic properties of the strain rate tensor will be analysed first with their possible implications for vorticity alignment (§ 2) before describing the averaging procedures and discussing the results (§§ 3 and 4). Furthermore, the average flow patterns will be compared with instantaneous turbulence in terms of the probability distribution of the invariants Q and R (§ 5) and the specific spatial arrangement of the coherent structures in the velocity vector field (§ 6). A possible dependence of the average patterns on the Reynolds number will be commented on (§ 6).

2. Analysis of possible flow patterns in principal strain coordinates

In the analysis of the strain rate tensor the concept of Mohr-circles (in analogy with the mechanical stress tensor, Gere & Timoshenko 1991) will be used, which yields a graphical representation of all admissible states of this tensor under a rotation of the coordinate system. It is based on geometric relations and applicable to any symmetric second-order tensor. Below, the diagonal components of the strain rate tensor will be referred to as the strain rates σ, representing the stretching rate of a filament instantaneously lined up with a coordinate axis, and the off-diagonal elements as rate of shearing τ, which is one-half the rate of angular change between two originally perpendicular filaments (with directions indicated by the indices). The Mohr-circles in the (σ, τ) plane (figure 2) are now a simple and useful tool to determine the maximum value of the off-diagonal elements in the strain rate tensor, and the direction for which this maximum occurs. Starting with the coordinate axes aligned with the principal

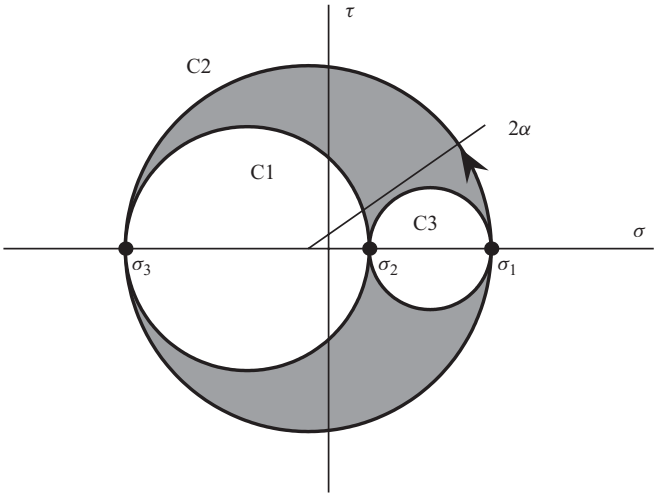

FIGURE 2. Mohr's circle for strain σ and shearing τ. See text for definitions.

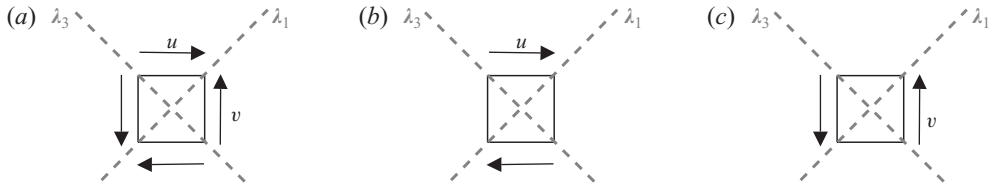

FIGURE 3. Three types of shearing motion around a square fluid element. The vectors indicate a relative velocity with respect to the fluid element. Also shown are the corresponding principal strain rate axes (dashed lines). (*a*) Pure strain ($u_y = v_x$), (*b*) shear layer ($v_x = 0$) and (*c*) shear layer ($u_y = 0$).

axes, the corresponding strain rate tensor has non-zero entries only along its diagonal, which are the principal strain rates σ_i. This state is represented by three points on the horizontal axis (figure 2). All other accessible states under a rotation of the coordinate system around the $\boldsymbol{\lambda}_2$ direction then collapse onto a circle (labelled 'C2') with its centre on the σ-axis at $(\sigma_1 + \sigma_3)/2$ and with radius $|\sigma_1 - \sigma_3|/2$. The angle of rotation α is also indicated in figure 2. Similar circles (labelled 'C1' and 'C3') can be constructed for rotations in the other directions starting from a coordinate system aligned with the principal axes. All possible combinations of shearing and straining are confined to the region enclosed by C2 and outside C1 and C3. It is now quickly seen that the maximum shearing (i.e. maximum off-diagonal element in $\boldsymbol{S}$) is obtained by a rotation over 45° in the plane spanned by the eigenvectors $\boldsymbol{\lambda}_1$ and $\boldsymbol{\lambda}_3$.

In fluid flow the shearing is composed of two velocity gradients, which can be unequal in magnitude (e.g. $\tau_{xy} = u_y + v_x$, note that the difference with shear *stress* is the viscosity). Hence, it can result from either a pure strain (which would be equivalent to a saddle point flow pattern, figure 3*a*) or a single component ($\tau_{xy} = u_y$ with $v_x = 0$ or alternatively $\tau_{xy} = v_x$ with $u_y = 0$, see figures 3*b* and 3*c*), which will be referred to as a shear-layer-type flow. The essential difference here is that shear layers contain vorticity, whereas a pure strain does not. Therefore, it is important at this point to establish which of these two flow types dominates in turbulent flow and to what extent. This is most relevant in the $\boldsymbol{\lambda}_1$, $\boldsymbol{\lambda}_3$ plane, as this plane contains the shearing

maximum and a shear-layer-type flow in that plane would relate to the component of vorticity in the direction of the intermediate eigenvector $\boldsymbol{\lambda}_2$.

3. Average flow field in the eigenframe of the strain rate tensor

3.1. *Averaging procedure*

To obtain the relative importance of a pure strain and a layered shear (figure 3), the average fluctuating velocity field on a grid aligned with the local principal strain directions is calculated. The averaging procedure can be summarized as follows. At a point in the measurement volume the principal directions of the strain rate tensor $\boldsymbol{\lambda}_i$ are determined. The positive orientations along these directions have to be chosen with some care as will be pointed out below. Then the velocity field around that point is resampled on a uniform rectangular grid with coordinates $(\lambda_1, \lambda_2, \lambda_3)$ along the corresponding local $\boldsymbol{\lambda}_i$ directions and the origin located at the considered point in the flow. Finally the resampled velocity fields for all points and for all realizations are averaged.

In order to differentiate between the pure strain and the layered shear in the $\boldsymbol{\lambda}_1$, $\boldsymbol{\lambda}_3$ plane an additional criterion for defining the positive $\boldsymbol{\lambda}_2$ direction is needed, because the shear-layer cases of figures 3(*b*) and 3(*c*) are equivalent in terms of the strain rate tensor and its eigenvectors. So when they occur, they will occur with equal probability in the eigenframe $\boldsymbol{\lambda}_i$ and average out to the pure strain case depicted in figure 3(*a*). This is a direct consequence of the strain rate field being symmetric in the eigendirections. Hence $\boldsymbol{\lambda}_i$ can be inverted without changing the strain rate field. To avoid averaging out the shear layers, the $\boldsymbol{\lambda}_2$ direction will be chosen such that its inner product with the vorticity vector is positive, which will collapse the case of figure 3(*c*) onto the case of figure 3(*b*). To maintain a right-handed system of coordinates, the first eigenvector is adapted accordingly. Note that this procedure is of no consequence to the case of pure strain (figure 3*a*). Further, since only two criteria (the definition of the positive direction along $\boldsymbol{\lambda}_2$ and $\boldsymbol{\lambda}_1$ as a function of $\boldsymbol{\lambda}_2$ and $\boldsymbol{\lambda}_3$) are used to reduce the original three degrees of freedom (one for each $\boldsymbol{\lambda}_i$ direction), the average patterns will have a remaining imposed symmetry about the line $\boldsymbol{\lambda}_2$. This, however, does not affect the relative contributions of pure strain and layered shear at the origin, which is our main interest at this point.

3.2. *Results*

The result of the averaging procedure for the TBL, channel flow and isotropic turbulence are shown in figures 4, 5 and 6, respectively. The pattern for isotropic turbulence represents the average over the complete computational domain, whereas for the boundary layer and channel flow only points at a specified distance from the wall are considered and averaging is performed in the (nearly) homogeneous directions parallel to the wall. These wall normal locations are in the outer layer between 0.13δ and 0.28δ, and at $0.2h$, where δ is the boundary-layer thickness and h is the channel half-height.

The averages share some pronounced and common features. First of all, near the origin in the λ_1, λ_3 plane (figures 4*a*, 5*a* and 6*a*) a flow compression and stretching are seen in the direction of the third and first eigenvector resulting in the shearing maximum when rotating the coordinate system by 45°, as expected. The local topology is a combination of pure strain and layered shear (as defined in figure 3), where the latter is observed to dominate the average flow pattern. This dominance will be quantified later on. The shearing is maximum in this plane, as shown above, and

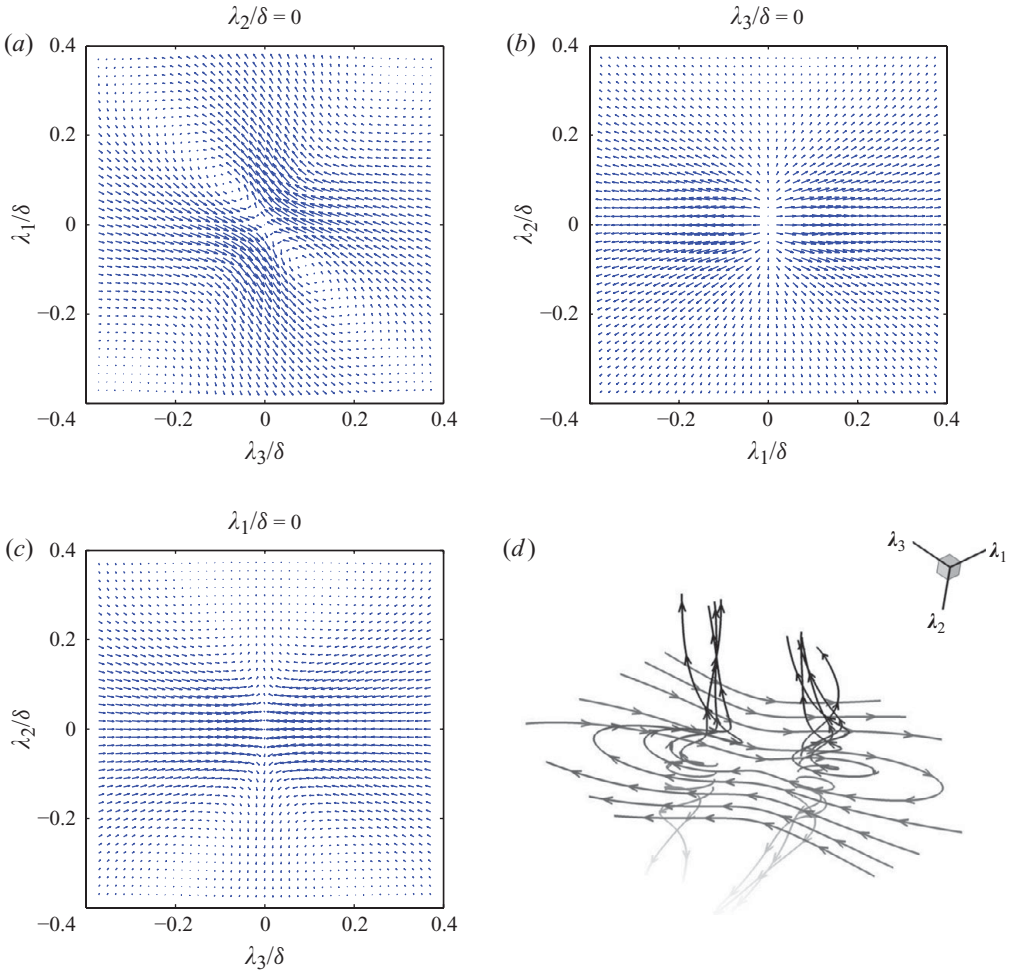

FIGURE 4. (Colour online) Average fluctuating velocity field in the coordinate system defined by the local principal strain directions for points between 0.13 and 0.28 δ distance from the wall in a TBL. The velocity vectors relative to the average velocity are shown in three cross-planes (*a–c*) with the corresponding 3D streamlines displayed in (*d*).

consequently it will yield a significant contribution to the vorticity vector in the $\boldsymbol{\lambda}_2$ direction, which provides an explanation for the observed preferential alignment of $\boldsymbol{\omega}$ with $\boldsymbol{\lambda}_2$. In this argument we have only used the observation that shearing is mainly asymmetric (of shear-layer type), which is a statistically dominant property of the turbulent flow as revealed by the averaged flow pattern in the eigenframe $\boldsymbol{\lambda}_i$. The alignment then follows directly from a geometric/kinematic consideration similar to Jimenez (1992). Additionally, the presence of saddles (pure strain without vorticity) and strong flow rotation may result in a non-perfect alignment of $\boldsymbol{\omega}$ with $\boldsymbol{\lambda}_2$. The effects of rotation will be discussed later in § 4.

Even though the above result may appear similar to the discussion of the alignment in a Burgers vortex sheet by Andreotti (1997), there is, however, a subtle difference in the fact that no (*a priori*) model flow is assumed in the present analysis. Hence it can be concluded here that shear layers not only *can*, but in fact *do* explain the alignment.

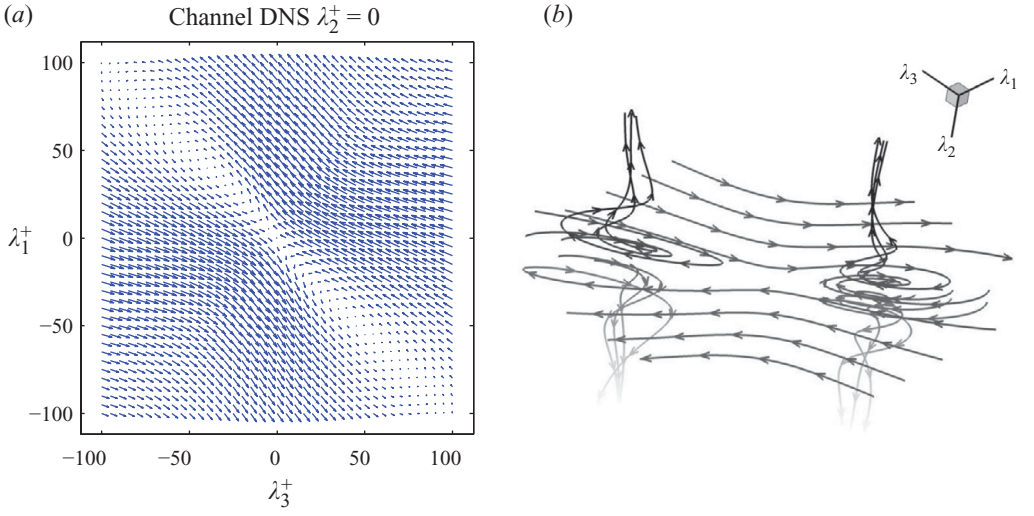

FIGURE 5. (Colour online) Average fluctuating velocity field in the coordinate system defined by the local principal strain directions for points at $0.2h$ distance from the wall in DNS channel data. The velocity vectors in the λ_1, λ_3 plane are relative to the average velocity (*a*). Note that 100 wall units is equal to $0.11h$. The corresponding 3D streamlines are displayed in (*b*).

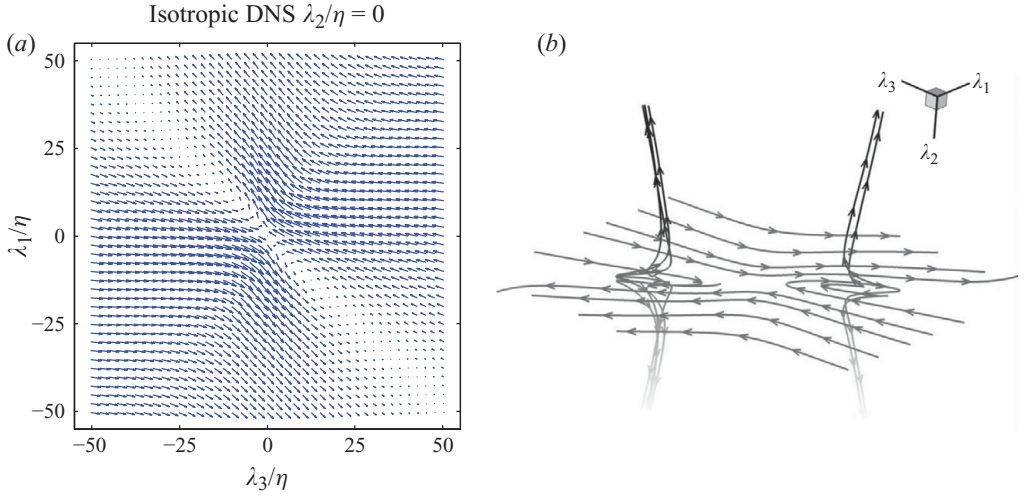

FIGURE 6. (Colour online) Average fluctuating velocity field in the coordinate system defined by the local principal strain directions for points in DNS of isotropic turbulence, shown as velocity vectors in the λ_1, λ_3 plane (*a*) and the corresponding 3D streamlines are displayed in (*b*).

Moreover, the present results suggest these are not simple shear layers, but may be composed of several aligned vortices. These shear layers appear to extend beyond a vortex diameter from the origin and, therefore, seem to be of a larger scale than the individual vortex itself, even when considering only one-half the symmetric pattern. We will return to that point in § 6.

A second common feature is the stretching in the direction of the intermediate eigenvector, which is expected as the intermediate eigenvalue σ_2 is widely reported to

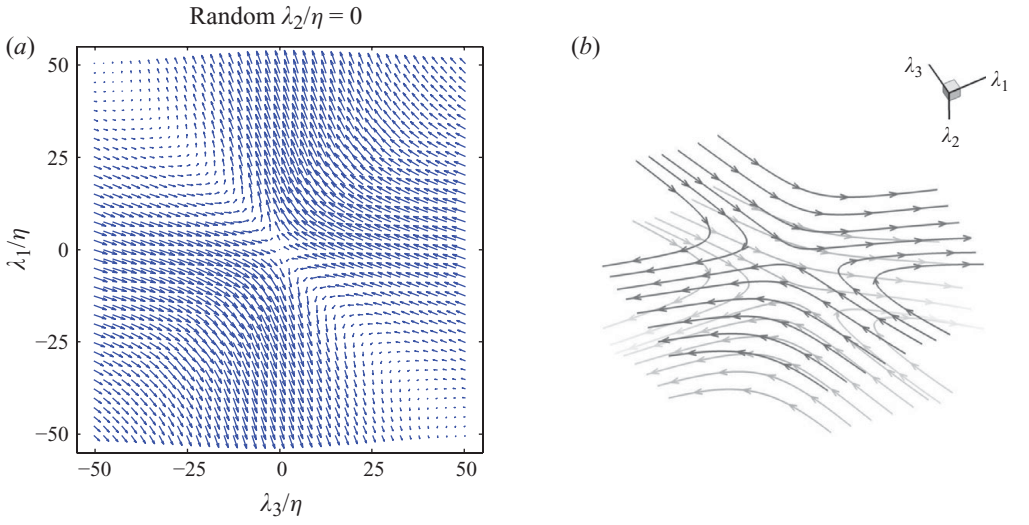

FIGURE 7. (Colour online) Average fluctuating velocity field in the coordinate system defined by the local principal strain directions for points in a random velocity field satisfying continuity, shown as velocity vectors in the λ_1, λ_3 plane (*a*) and the corresponding 3D streamlines are displayed in (*b*). The velocity power spectrum is equal to the isotropic turbulence case presented in figure 6 as is η.

be positive on average. Consequently, the flow pattern in the λ_1, λ_2 plane and λ_2, λ_3 plane reveal a node and a saddle, respectively (see figure 4*b–c* for the TBL with very similar patterns obtained for the other cases, which therefore have been omitted). This also means that the vorticity in the mentioned shear layer in the λ_1, λ_3 plane is stretched, which is required on average to balance viscous dissipation in statistically steady turbulence.

It is now of interest to visualize the streamlines in the averages and look at the flow topology in the shear layers in some more detail. Three-dimensional renderings of the streamlines are presented in figures 4(*d*), 5(*b*) and 6(*b*), where the greyscale intensity is proportional to the λ_2 coordinate. Two distinct stable foci representing stretched vortices are visible in each plot. They are located within the shear layer on opposite sides from the origin, as expected due to the symmetry imposed by the averaging process. Within the foci, the streamlines spiral inwards while moving away in the positive or negative λ_2 direction. The topology at the origin is that of an unstable node with streamlines quickly moving away from that point, which cannot be visualized adequately, but instead may be inferred from the corresponding vector plots. Furthermore, the shear layer separates two relatively larger-scale quasi-uniform flow regions having opposing velocity directions. In these regions the streamlines are nearly parallel. The average flow patterns are remarkably similar for the different flow cases. They also bear great similarity with the flow features in the instantaneous turbulent flow fields, which will be elaborated upon in § 6.

In order to demonstrate that the presented patterns are not trivial results, the averaging procedure has been applied to a random velocity field, which is divergence free and has the same velocity power spectrum as the isotropic turbulence case but with a randomized phase. It has been generated using the method described in Rogallo (1981). The difference with real turbulence is best seen from the streamlines in the average flow pattern for the random velocity field (figure 7*b*), which reveals

a skewed saddle point topology at various λ_2 locations (indicated by the grey scale). This result is in sharp contrast with the shear layer with stable foci in real turbulence. Furthermore, there is no stretching along the λ_2-axis for the random field, as can be inferred from the streamlines.

Additionally, the averaging procedure is also tested on the Burgers vortex flow, which is known to have $\boldsymbol{\omega}$ alignment with $\boldsymbol{\lambda}_2$ in the periphery around the core (but not in the actual inner core itself) and therefore it has been used to explain this alignment in the past. The flow is a solution of the Navier–Stokes equations and represents a stretched vortex with velocity components:

$$\frac{-r^*}{2Re}, \quad \frac{2(1-\exp(-r^{*2}/4))}{r^*}, \quad \frac{z^*}{Re} \tag{3.1}$$

in the radial, angular and axial direction, respectively, where r^* and z^* are non-dimensional radial and axial coordinates and Re is a Reynolds number representing the amount of vorticity stretching relative to the peak vorticity. Increasing Re in this case corresponds to decreasing stretching. The vortex core diameter D, defined as twice the radial distance for the angular velocity peak, is about 4.5 non-dimensional lengths, which will be used to normalize the lengths. The average pattern in the strain rate eigenframe for a single vortex at $Re = 5000$ is presented in figure 8(a) revealing four vortices in a symmetric arrangement with a saddle point topology in between, which is clearly different from any of the patterns shown before for actual turbulence. Here, the flow has been averaged over a box centred on the vortex core spanning $4.4D$ in axial direction and $8.9D \times 8.9D$ in the other directions. Averaging over much smaller domains (not shown), of the order of one core diameter, which would be smaller than the expected distance between separate vortices in turbulence, returns a different pattern of two vortices along a diagonal line with a large-scale swirling motion around them instead of an extended shear layer as before. Further, while increasing Re does not change the result qualitatively, decreasing Re, thereby increasing the vortex stretching, yields again a large-scale saddle point flow (figure 8c) similar to the random velocity field (figure 7). Finally, a field of 100 Burgers vortices randomly positioned with an average spacing of $2.0D$ and having random swirling directions results, for high Re, in two vortices with a large-scale swirl enclosing them (figure 8b). The two vortices inside appear to be separated along the diagonal by approximately the average spacing ($2.0D$). For lower Re the average is again a saddle point (figure 8d) with the transition in topology occurring between $Re = 5000$ and 500. This is an interesting result as one may expect a lower, order unity, Re to be more representative of small-scale turbulence (where peak vorticity and stretching are of similar order), but instead the corresponding average pattern reveals the largest difference with respect to real turbulence. This is yet another indication that Burgers models can offer only a partial explanation for the features of small-scale turbulence. But more importantly, the absence of a larger-scale shear layer in all these simulations demonstrates this feature is not introduced by the applied averaging procedure or the particular reference frame, hence must be attributed to real turbulence.

The relative importance of layered shear versus pure strain (i.e. saddle) can be quantified by evaluating the velocity gradient tensor at the origin in the average flow patterns. This is done in a new coordinate system (t, n) with corresponding velocity components V_t and V_n, where n is the distance normal to the shear layer and t is taken along the shear layer in the λ_1, λ_3 plane (this is equivalent to a 45° rotation around the λ_2 axis, figure 9). The velocity gradient tensor $\boldsymbol{A}$ then takes on the

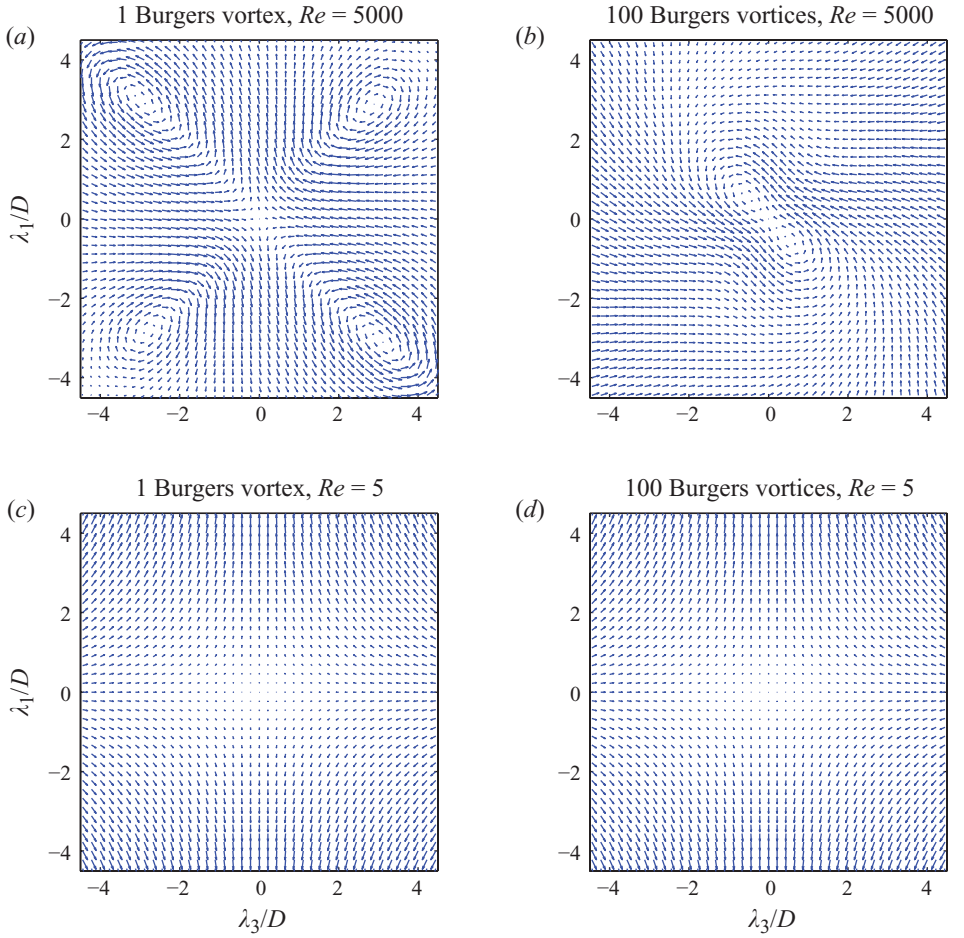

FIGURE 8. (Colour online) Average fluctuating velocity field in the coordinate system defined by the local principal strain directions for a single Burgers vortex at $Re = 5000$ or 5 (*a*, *c*) and a field consisting of 100 randomly positioned Burgers vortices all at $Re = 5000$ or 5 (*b*, *d*). The velocity vectors are shown in the λ_1, λ_3 plane ($\lambda_2 = 0$).

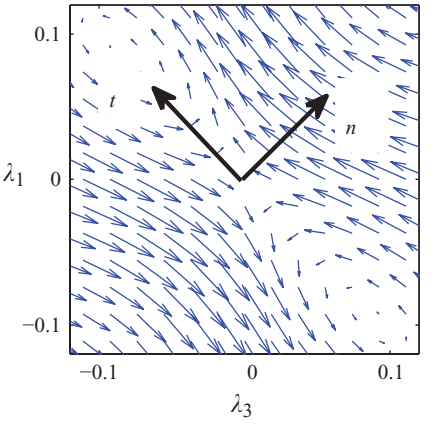

FIGURE 9. (Colour online) Definition of the *t*, *n* coordinate system with the strain rate eigenframe.

	PIV TBL	DNS channel	DNS isotropic	Random
Shearing in (λ_1, λ_2, λ_3) fields (§ 3)				
Part due to pure strain (saddle)	40 %	29 %	36 %	51 %
Part due to shear layer	60 %	71 %	64 %	49 %

TABLE 1. Overview of results in the eigenframe of the strain rate tensor.

form:

$$\boldsymbol{A} = \begin{bmatrix} \partial V_t/\partial t & 0 & \partial V_t/\partial n \\ 0 & a_{22} & 0 \\ \partial V_n/\partial t & 0 & \partial V_n/\partial n \end{bmatrix}, \tag{3.2}$$

where a_{22} is the velocity gradient in the λ_2 direction. The total shearing can then be defined as $(\partial V_t/\partial n + \partial V_n/\partial t)$. Note that both terms are positive and that $\partial V_t/\partial n > \partial V_n/\partial t$ as a consequence of the chosen coordinate system (figure 9). Furthermore, the total shearing is assumed to be composed of a symmetrical component $2\partial V_n/\partial t$ and an asymmetrical component $(\partial V_t/\partial n - \partial V_n/\partial t)$, which, when normalized by the total shearing, correspond to a relative contribution from a pure strain and a shear layer, respectively. Note that the asymmetric component is equal to the vorticity. These relative contributions are presented in table 1 for all turbulent flows considered as well as for the random velocity field. The shear-layer contribution is found to be 60–70 % of the total shearing in real turbulence, whereas it is only 50 % in a random field. The smallest value is attained for the TBL, which is likely due to the larger flow scales measured in that particular PIV experiment compared to the high resolution DNS for the other flows. Still the agreement between experiments and numerical simulation is good. To check for a possible bias towards the stronger shear events in the above results, a slightly modified averaging procedure was employed in which each individual resampled velocity field is normalized by the local total shearing prior to the averaging step. The relative contribution of a layered shear in that case is 64 % for the TBL case, which is close to the 60 % without normalization (table 1). This suggests the above results are not significantly biased and are representative of strong as well as weaker total shearing events.

4. Average flow pattern around the vorticity and swirl vector

Following a procedure similar to the above (§ 3.1), the average flow field around the vorticity $\boldsymbol{\xi}_\omega$ and the swirl $\boldsymbol{\xi}_{swirl}$ directional vector is determined, and the results for the TBL are shown in figure 10. The swirl vector exists only when the velocity gradient tensor $\boldsymbol{A}$ has two complex eigenvalues (Zhou *et al.* 1999) and is defined here as the direction of the eigenvector corresponding to the remaining real eigenvalue of $\boldsymbol{A}$. In these averages a second direction $\boldsymbol{\xi}_3$ is defined as the projection of the third eigenvector of the strain rate tensor $\boldsymbol{\lambda}_3$ onto to the plane normal to $\boldsymbol{\xi}_\omega$ or $\boldsymbol{\xi}_{swirl}$. This is motivated by the observation that $\boldsymbol{\xi}_\omega$ is predominantly oriented normal to $\boldsymbol{\lambda}_3$ (see figure 1). The remaining direction $\boldsymbol{\xi}_1$ is then chosen such as to produce a right-handed rectangular coordinate system (ξ_1, ξ_w, ξ_3) or $(\xi_1, \xi_{swirl}, \xi_3)$. As before, the fluctuating velocity is resampled in this local coordinate system for each point in the flow, and this is then averaged over all the points considered. The results obtained

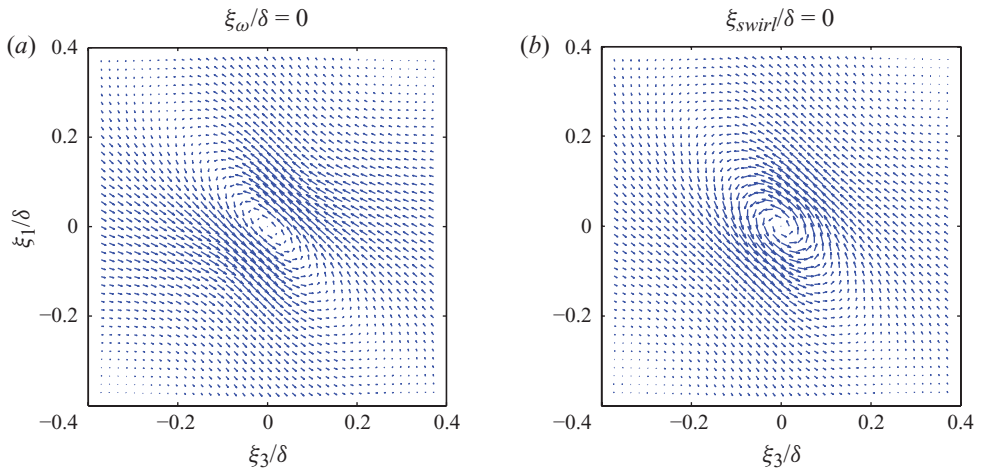

FIGURE 10. (Colour online) Average fluctuating velocity field in the coordinate system defined around the vorticity direction $\boldsymbol{\xi}_\omega$ (*a*) and swirling direction $\boldsymbol{\xi}_{swirl}$ (*b*) in a TBL. The velocity is relative to the average velocity. See text for the definition of the other axis.

for the different turbulent flows are very similar, and the conclusions reached here are applicable to all the cases considered in this study.

The average flow around the vorticity vector in the TBL (figure 10*a*) reveals the superposition of a shear layer and a perfectly circular rotational motion, which is defined as a rotationally symmetric swirling topology, for example $u_y = -v_x$. The result shows that the flow pattern around the vorticity vector is mainly associated with shear layers and to a lesser extent with such a rotationally symmetric swirling motion. This may appear to contradict the conclusions of She *et al.* (1990), Jimenez *et al.* (1993) and others, who report that vorticity is concentrated in (vortex) tubes. However, if the vortices align, as observed in the average flow pattern in the eigenframe of the strain rate tensor (figures 4–6) and in the instantaneous flow visualizations of Jimenez *et al.* (1993) and Vincent & Meneguzzi (1994) in isotropic turbulence, then that would explain both results. Furthermore, the result here showing that the contribution of a *rotational symmetric* swirling motion to the vorticity is weak, means that the alignment of vorticity $\boldsymbol{\omega}$ and the intermediate eigenvector $\boldsymbol{\lambda}_2$ can be explained by the previous average flow pattern in the eigenframe of the strain rate tensor (vorticity related to shear layers is captured in the results of § 3 and the expected deviations due to a symmetric rotation are shown to be small here). The presence of vortices in a shear layer also explains why the vorticity alignment can be found in the inner core region of intense vortices, which is not the case in models like the Burgers vortex (Andreotti 1997).

In the other planes containing the vorticty direction (not shown), the average flow around the vorticity vector resembles a saddle and a node, similar to the results of figure 4. Again, vorticity is found to be stretched on average. Also as before, the flow pattern appears coherent up to 0.2δ–0.3δ distance from the origin with relatively uniform flow conditions on either side of the shear layer.

In contrast, the flow around the swirling direction displays hardly any evidence of vortex stretching in the direction of ξ_{swirl}. As can be seen from figure 11, the swirling direction is predominantly aligned with the first (maximum stretching) and third (maximum compression) eigenvector of the strain rate tensor. The averaging

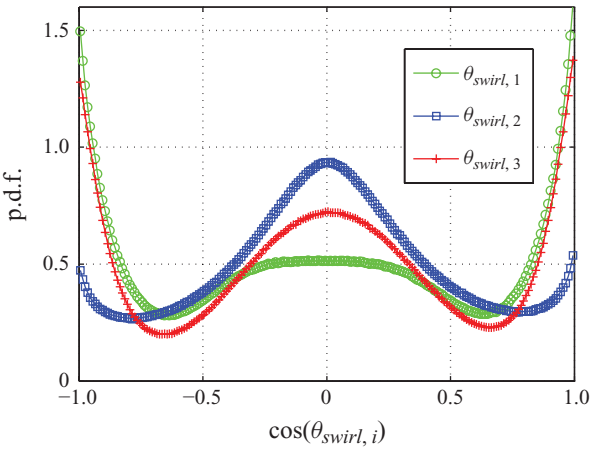

FIGURE 11. (Colour online) Probability density functions of the cosine of the angle between the swirl direction and the eigendirections of the strain rate tensor.

procedure cancels out both stretching and compression. The different preferential orientation with respect to the eigenvectors can be explained as follows. Swirling motion is (nearly) rotational-symmetric hence the two eigenvalues related to the eigenvectors in the plane approximately normal to the swirling direction have the same sign. Because the sum of the eigenvalues equals zero, the remaining eigenvalue, related to the eigenvector in the swirling direction, must be of opposite sign and consequently must represent either maximum stretching or compression. These results again confirm that vorticity and a vortex (defined as a swirling motion around $\boldsymbol{\xi}_{swirl}$) are not the same thing. Still the average swirling motion appears to be imbedded in a shear-layer environment (figure 10*b*). It is therefore conjectured that the swirling motion is the result of a shear-layer roll-up (see e.g. Passot *et al.* 1995). During the roll-up the orientation of the coordinate system defined by the eigenvectors of the strain rate tensor $\boldsymbol{\lambda}_i$ may flip due to changing magnitude, hence the order, of the eigenvalues. The switching of the eigenvectors has been observed in the experiments of Guala *et al.* (2005).

To quantify the relative contributions of layered shear and rotationally symmetric swirling to the total vorticity at the origin in the average flow in the coordinate system (ξ_1, ξ_w, ξ_3) (figure 10*a*), the velocity gradient tensor $\boldsymbol{A}$ is again evaluated in the (t, n) system of reference (where t is taken in the direction of the shear layer and n is normal to it, similar to figure 9). As before, $\boldsymbol{A}$ takes on the form of (3.2), however this time $\partial V_t/\partial n > -(\partial V_n/\partial t) > 0$. The total vorticity magnitude is then given by $(\partial V_t/\partial n - \partial V_n/\partial t)$, which is split into a contribution from symmetric rotation (defined as $-2\partial V_n/\partial t$) and a remaining part $(\partial V_t/\partial n + \partial V_n/\partial t)$ representative of a layered shear (note that the latter corresponds to the asymmetric part of vorticity and that the plus sign in this case is only the result of the negative $\partial V_n/\partial t$ and positive $\partial V_t/\partial n$). For the TBL (figure 10*a*), this yields relative contributions to the total vorticity of 25 % (rotation) and 75 % (shear layer). The ratios for the other turbulent flows are listed in table 2. The DNS results indicate an even larger percentage due to layered shear (>80 %), which is likely due to the small flow scales resolved. These percentages are very different for the random velocity field, which returns a 50–50 % balance between layered shear and rotation. This is yet another indication that the reported average

	PIV TBL	DNS channel	DNS isotropic	Random
Vorticity in (ξ_1, ξ_ω, ξ_3) fields (§ 4)				
Part due to rotation	25 %	17 %	18 %	49 %
Part due to shear layer	75 %	83 %	82 %	51 %

TABLE 2. Overview of results in the eigenframe around the vorticity vector.

flow patterns for real turbulence are not trivial and contain an excess of layered shear with respect to the random field results.

5. Invariants of the velocity gradient tensor

The topological details of the average flow patterns in the eigenframe of the strain rate tensor (§ 3) will be explored further by evaluation of the invariants Q and R of the velocity gradient tensor. From this a Q, R scatter plot is produced containing all points within the average pattern. The invariants are normalized using $\langle Q_W \rangle$, which is the average value of the second invariant of the rate of rotation tensor, i.e. the asymmetric part of the velocity gradient tensor $(\boldsymbol{A} - \boldsymbol{A}^T)/2$. The normalization, however, is not important in the qualitative discussion that follows.

The resulting scatter plots are shown in figure 12 for the TBL, channel flow, isotropic turbulence and the random velocity field. All plots reveal a concentration of points near $Q = R = 0$, which correspond to the points away from the origin in the average flow pattern, where the velocity gradients are relatively small. The results also show an important difference between real turbulence and the random velocity field for the points having a relatively large velocity gradient (i.e. points further away from $Q = R = 0$). Whereas the random field returns a scatter symmetric in R with the largest velocity gradients occurring in node-saddle topologies, which are the points below the dashed, null discriminant line (Chong *et al.* 1990), real turbulence does not display such symmetry far away from $Q = R = 0$. Rather we observe an accumulation of points in the $Q > 0$, $R < 0$ corner (labelled I in figure 12*a*) and the $Q < 0$, $R > 0$ corner (labelled II), which correspond to stable foci and unstable node-saddle topologies, respectively (Chong *et al.* 1990). As has been shown in § 3, both these stable foci and unstable node-saddle occur within the shear layer in the average flow patterns (see figures 4–6).

The QR scatter plots for the average patterns are consistent with the symmetry breaking that has been found in the joint p.d.f.s of Q and R for various instantaneous turbulent flow fields, for which iso-contours display a teardrop shape with the tail along the right branch of the null-discriminant line into region II and the body inclined towards region I (Soria *et al.* 1994; Blackburn *et al.* 1996; Ooi *et al.* 1999; Chong *et al.* 1998; Elsinga & Marusic 2010). Hence, the presented patterns can be the underlying flow feature explaining the inclination of the QR joint-p.d.f. contours in turbulent flows. The exact teardrop shape could then follow from (small) variations of the flow pattern around the average. One can think of variations in vorticity magnitude and stretching rates as well as variations in the spatial separation of the different local topologies.

In the above scenario the joint p.d.f. is not simply a pointwise statistic, but has meaning in terms of an extended coherent flow pattern. This seems to be supported further by previous observations revealing that from the basic state $Q = R = 0$, representing degenerate topologies including shear layers, all topology types develop (Elsinga & Marusic 2010). Then from topological constraints it follows that those

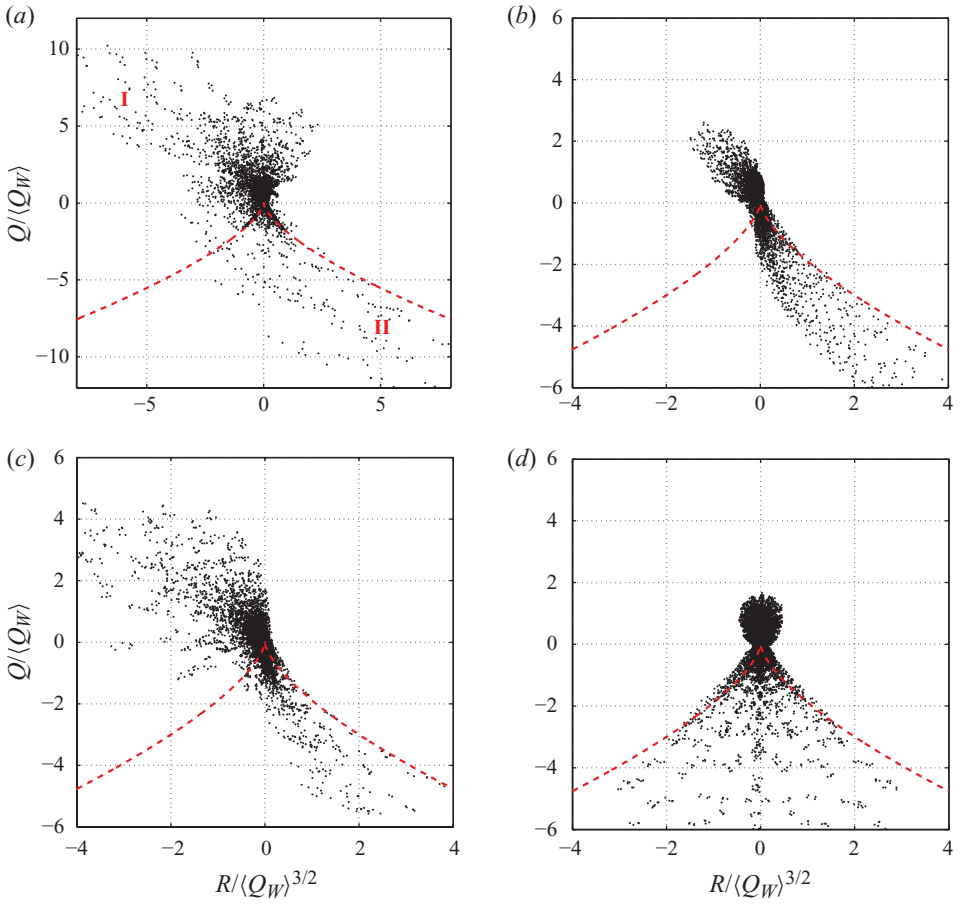

FIGURE 12. (Colour online) QR scatter plot for the conditional averages in the strain rate tensor eigenframe (figures 4–7). The dashed line indicates the null discriminant line separating focal topologies (above the line) from node-saddle topologies (below the line). (*a*) PIV TBL, (*b*) DNS channel, (*c*) DNS isotropic turbulence and (*d*) Random field.

focal and nodal topologies must be created at the same time in statistically steady turbulence. This shows the different topologies are strongly linked.

6. Discussion

6.1. *Observations of the average pattern in instantaneous turbulence*

It is natural to ask how relevant the average fluctuating velocity patterns in the strain rate tensor eigenframe (figures 4–6) are in relation to the instantaneous flow. Are they an artifact of the averaging process or do they represent actual patterns frequently occurring in real turbulence?

For the case of wall-bounded turbulence, such as the TBL, channel and pipe flow, extended regions of relatively uniform streamwise fluctuating flow velocity, u, have widely been observed in the outer layer starting from Meinhart & Adrian (1995). These regions can be very long in the streamwise direction ($>10\delta$) compared to their typical spanwise dimension ($\sim 0.5\delta$) and although they tend to meander, they

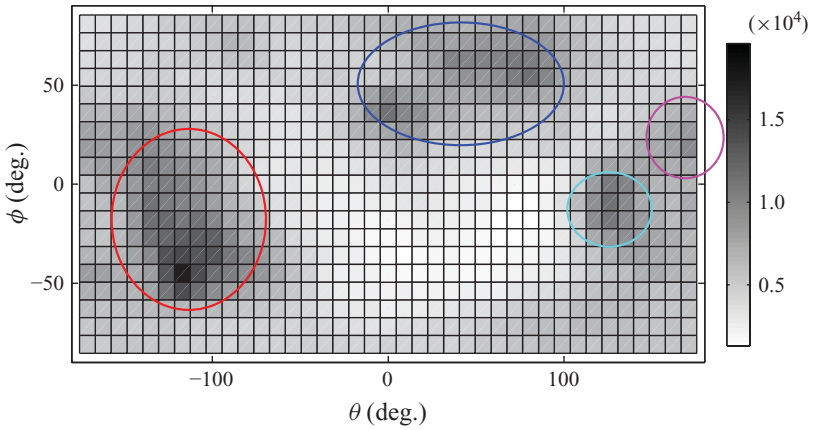

FIGURE 13. Number density of velocity vector directions in a subvolume of the isotropic turbulence divided by $\cos(\phi)$. θ represents the azimuth angle in the x, y plane, while ϕ is the elevation angle with respect to the x, y plane.

are predominantly oriented in the streamwise direction making them easy to detect in hotwire and planar velocity measurements (Hutchins & Marusic 2007; Monty *et al.* 2007). These regions of quasi-uniform streamwise velocity are separated by thin shear layers commonly containing several vortices (of hairpin type) that convect at approximately the same velocity. This observation has lead to the formulation of the hairpin packet model for the outer layer structure in wall-bounded turbulence (Adrian, Meinhart & Tomkins 2000), in which several hairpins are aligned in the streamwise direction enclosing a region of nearly uniform low-speed flow. The packet model has subsequently been supported by flow visualizations of 3D velocity data from DNS and experiments (Adrian & Liu 2002; Ringuette, Wu & Martin 2008; Elsinga *et al.* 2007, 2010) as well as by their signatures observed in planar PIV measurements (Ganapathisubramani, Longmire & Marusic 2003; Tomkins & Adrian 2003). The flow structure in the reported packets is very similar to the present average patterns in the strain rate eigenframe, i.e. a shear layer separating uniform flow regions and containing foci or vortices. Additionally, del Alamo *et al.* (2006) have estimated the fractal dimension of vortex clusters in the logarithmic region to be 2, which suggests again an organization of vortices on surfaces or sheets.

The existence of large-scale uniform velocity zones in isotropic turbulence is arguably less well known due to the lack of a principal direction and associated visualization difficulties. Although there have been reports of the alignment of some vortices (Vincent & Meneguzzi 1994) and the background vorticity being concentrated in sheets with the tube vortices embedded in this background (Jimenez *et al.* 1993), which are based on a visual inspection of their DNS data. Results from a box-counting method (Moisy & Jimenez 2004) have also revealed a non-uniform distribution of intense vorticity and strain-rate structures, which indicates the presence of a large-scale organization of these small-scale structures without detailing its nature.

A first indication of uniform velocity zones in the present isotropic turbulence data is given by the number density for the velocity direction angles as shown in figure 13, where θ represents the azimuth angle of the velocity vector in the x, y plane and ϕ is the elevation angle with respect to the x, y plane. For the plot only velocity vectors are considered within a subvolume spanning one-fifth of the total volume, i.e.

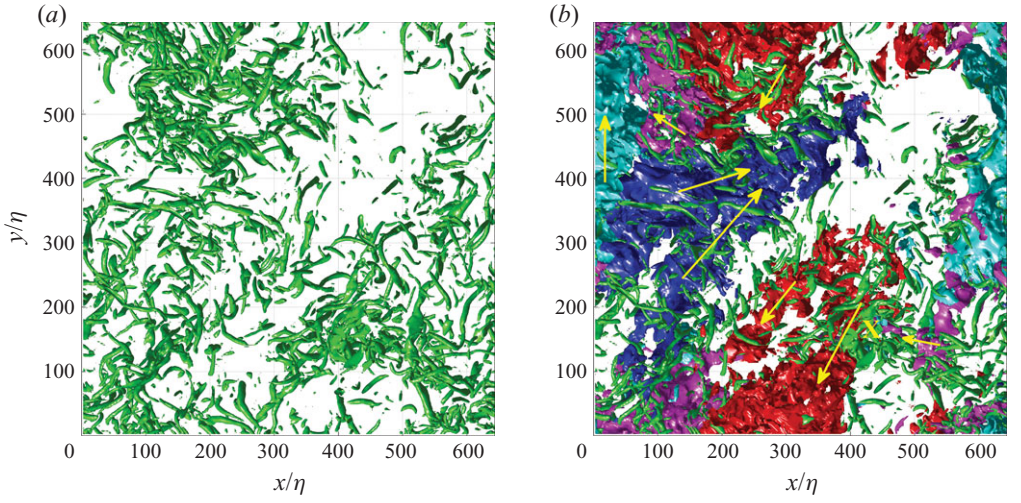

FIGURE 14. Visualization of the intense vortical structures in a subvolume of isotropic turbulence (green) without (*a*) and with (*b*) a number of uniform velocity zones (blue, red, cyan and magenta depending of the flow direction as indicated by the arrows).

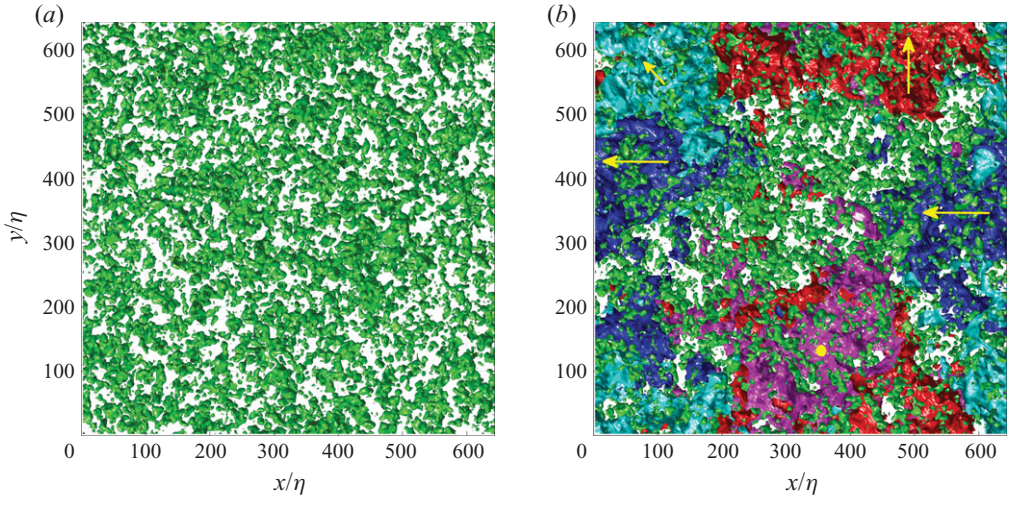

FIGURE 15. Same as figure 14 but for a random velocity field.

$256 \times 256 \times 50$ points corresponding to $644\eta \times 644\eta \times 125\eta$. Several distinct principal flow directions marked by an increased probability may be detected in figure 13, four of which are indicated by ellipses. The spatial structure associated with these four flow directions is visualized using an indicator function, which is non-zero only when the velocity direction is within one of the ellipses (figure 13) and its magnitude is above a given threshold (1.3 times the root mean square (r.m.s.) of the u-component of velocity here). These detected structures in the subvolume are shown in figure 14(*b*) in colours corresponding to those of the ellipses in figure 13. For clarity, yellow arrows have been added to indicate the approximate average flow direction. Note the extended spatial coherence of the detected regions in the direction of their velocity, which is of the order of the computational domain. Within each region the flow direction and

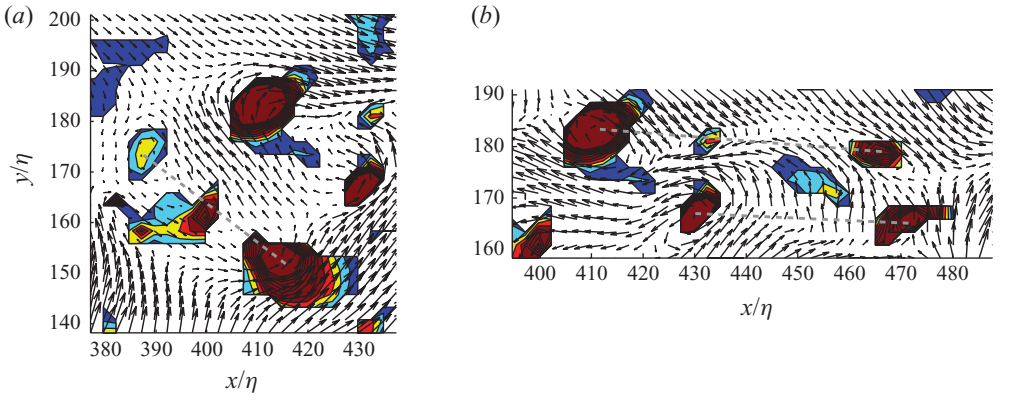

FIGURE 16. (Colour online) Details of the isotropic turbulence field near the position marked X in figure 14. The contours indicate positive levels of the second invariant of the velocity gradient Q to detect swirling motion or vortices. Furthermore, a convective velocity has been subtracted from the velocity vectors to highlight the flow relative to the vortices.

velocity magnitude is relatively constant (above the threshold), hence they may be regarded as uniform flow regions. Also shown in green in figure 14 are the intense vortical structures detected using the second invariant of the velocity gradient tensor Q (the threshold is 1.6 times the r.m.s. of Q), which have the well-known tube or worm like shape (She *et al.* 1990; Jimenez *et al.* 1993). As in Vincent & Meneguzzi (1994) alignment of intense vortices can be observed in figure 14(*a*) showing only the vortices, which is even clearer when plotting the vortices together with the uniform flow regions (figure 14*b*). The latter plot further suggests that the vortices are predominantly found near the edges of the uniform flow regions consistent with a model of aligned vortices separating the large-scale motions. In comparison, a random divergence free velocity field does not reveal this level of organization (figure 15) even if the velocity power spectrum and method of visualization are identical to the isotropic turbulence field. For the random field, the uniform flow regions are more round and not elongated. Furthermore, the vortices are blob like and appear uniformly distributed throughout the volume, which is very different from the observed alignment around the uniform flow regions in the case of isotropic turbulence.

Figure 14 also contains clusters of vortices, which are not easily interpreted using the present method of display. One example, labelled X in figure 14(*b*) (near $x/\eta = 400$, $y/\eta = 200$), is examined more closely using the detailed visualizations in figure 16. These show velocity vectors in the x, y plane, which is approximately normal to the axis of the vortices visible in this plane. These vortices are shown by the contours of positive Q. Further, note that a convective velocity has been subtracted to highlight the flow pattern relative to the vortices. Figure 16(*a*) shows three vortices aligned along the dashed line convecting at approximately the same velocity, which is assumed to be equal to the flow velocity inside the vortex core. Between the vortex cores saddle points are found. On either side of the dashed line the flow appears relatively uniform and without vortical motion. Similar patterns are observed in figure 16(*b*), where two dashed lines indicate the alignment of two and three vortices separating larger regions of more uniform flow. These results demonstrate that vortex alignment also occurs at a smaller scale containing only a few vortices as compared to the large scale in figure 14.

Based on the above results and similar observations reported in the literature, it is concluded that the pattern of aligned vortices separating large-scale uniform flow

	PIV TBL	DNS channel	DNS isotropic
Taylor microscale	0.18δ ($\sim 29\eta$)	76^+ (24η)	26η
Distance between vortex cores	0.26δ ($\sim 42\eta$)	130^+ (41η)	46η

TABLE 3. Taylor micro length scale compared to the distance between vortex cores in figures 4–6.

regions is common in instantaneous realizations of both wall-bounded turbulence and isotropic turbulence, which strongly supports the idea that the presented average pattern in the strain rate eigenframe (figures 4–6) is representative of a general frequently occurring flow pattern. Moreover, in view of these patterns having a strong link with universal aspects of turbulence, such as the vorticity alignment (§ 3) and the teardrop shape of the joint p.d.f. of the invariants Q and R (§ 5), it is believed that quasi-uniform flow regions separated by shear layers containing the (intense) vortical structures also are a universal aspect of developed turbulence in general. Turbulence, however, is not a simple collection of these average patterns (randomly) distributed in space. Rather, the averages should be viewed as a synthesis of turbulence, which contains features/patterns that occur very frequently in the instantaneous turbulent velocity fields. They are the dominant pattern so to say.

6.2. *A possible Reynolds number scaling and a model for turbulence*

The average patterns in the strain rate eigenframe (figures 4–6) contain features that may be associated with the length scales of turbulence, i.e. the Kolmogorov length scale, η, the Taylor microscale, l_t, and the integral length scale, L, which allows us to speculate on a Reynolds number scaling for these patterns according to $\eta/L = Re^{-3/4}$ and $l_t/L = Re^{-1/2}$. The diameter of the vortex cores in particular, but also the thickness of the shear layers, are currently believed to scale on the Kolmogorov length scale (Jimenez *et al.* 1993; del Alamo *et al.* 2006; Ganapathisubramani, Lakshminarasimhan & Clemens 2008), where the average core diameter is found to be around 10η. The uniform opposing motions on either side of the shear layer are typically large-scale motions, and hence they have an associated length scale L. Lastly, the distance between neighbouring vortices is proposed to be of Taylor microscale order, consistent with the dimensions of the dissipation structures observed between the vortices (Ganapathisubramani *et al.* 2008). Although the actual vortex core may be of η size, the influence of the vortex may thus extend over distances of l_t. To provide some support for this scaling, the Taylor microscale has been estimated for the present flow cases using $l_t = \sqrt{\overline{u^2}/\overline{u_x^2}}$ and compared to the distance between vortex cores in the average patterns (taken as the distance between the points of zero velocity inside each swirl region in figures 4*a*, 5*a* and 6*a*). The results (table 3) are consistent with the proposed scaling and suggest a vortex spacing of $1.7l_t$. We should note, however, that due to the limited separation between η and l_t scales, higher-Reynolds-number data would be required to further confirm the proposed scaling of the vortex spacing. Also, the Taylor scale for the experimental boundary-layer data should be taken as indicative due to the limited spatial resolution in this measurement, which is expected to lead to a slight underestimation of the velocity gradients and consequently overestimation of the Taylor microscale.

The present results further suggest a universality of the small-scale turbulent motions when studied in an appropriate local frame of reference, which is taken here

as the eigenframe of the rate of strain tensor. The concept of small-scale universality is hardly new. However, less well known are the (spatial) relation between the small- and large-scales of motion and also what would be a suitable reference frame. (Although, a local frame of reference is in fact implicit in the analysis of local flow topology through the invariants of the velocity gradient tensor Q and R.) The observed small-scale universality may be used to formulate a general model for the organization of flow structures, in which shear layers are folded around large-scale uniform momentum flow. These shear layers contain the topological features, and hence topology dynamics, with the Reynolds number scaling as discussed above. The proposed universal organization gives rise to the conjecture that differences between various types of turbulence simply lie in the character of the shear layers (folded/unfolded/random or not) possibly associated with large-scale instability modes of the various flows prescribing the nature of the large-scale uniform flow regions. Alternatively, it can be argued that the vortices align themselves thereby producing the large-scale motions. In the instantaneous velocity field the result is the same, and therefore a distinction cannot be made on the basis of the present data. This would require further study of the temporal evolution of the flow structures, such as for instance shear-layer roll-up (Ruetsch & Maxey 1992; Vincent & Meneguzzi 1994), which is outside the scope of the present work. More generally, it can be said that the difference between isotropic and non-isotropic turbulence is caused by statistical differences in the alignment of the eigenframe with respect to the fixed world coordinates x, y, z.

The suggested direct link between small and large scales has implications for large-eddy simulations (LES), where the large scales are resolved and the smaller flow scales have to be modelled. In particular, the dependence of the orientation and organization of the latter on the large scales provides further support for a subgrid modelling based on coherent structures as for instance proposed by Misra & Pullin (1997).

Additionally, the proposed flow organization is consistent with some other observations regarding small-scale turbulence. First, the relatively thin shear layers containing vortices are consistent with the intense small-scale intermittency (Batchelor & Townsend 1949). Secondly, the large instantaneous dissipation, $\varepsilon = 2\nu S_{ij}S_{ij}$, occurs in the node-saddle-saddle topologies in between the aligned co-rotating vortices within the shear layer and it is sheet-like (see figures 4–6), which has also been reported before (e.g. Chacin & Cantwell 2000; Moisy & Jimenez 2004; Ganapathisubramani *et al.* 2008). There may also exist a connection between the shear layers within turbulent flows and the turbulent/non-turbulent interfaces, which have discontinuities in velocity and a tendency towards a singularity in the mean vorticity, as recently shown by Westerweel *et al.* (2009). A shear layer located at the interface can explain these observations, and it is quite possible that this layer has a similar internal structure consisting of aligned vortices to that we report here.

6.3. *Dynamics*

Concerning the origin of sheet structures in turbulence, analysis of the vorticity equation, assuming the nonlinear and viscous terms to be small and straining to be much larger than vorticity, has shown that vorticity tends to produce sheets possessing the vorticity alignment with the intermediate eigenvector of the rate of strain tensor (Kevlahan & Hunt 1997). Similarly, Betchov (1956) proposed that vorticity forms sheets when the intermediate eigenvalue of the strain rate tensor is positive. Following its formation, shear-layer roll-up has been observed by several

researchers (e.g. Ruetsch & Maxey 1992; Vincent & Meneguzzi 1994; Passot *et al.* 1995). This dynamic sequence of events leading to the aligned vortex pattern may have aspects in common with transitional flows, where shear layers associated with low-speed streaks in early (by-pass) transition become unstable leading to small-scale vortex formation (Swearingen & Blackwelder 1987; Brandt, Schlatter & Henningson 2004). It underlines again the significance of shear layers in turbulence.

7. Conclusions

The flow topology associated with universal aspects of small-scale turbulence has been investigated by evaluating the average flow pattern in the eigenframe defined by the eigenvectors of the rate of strain tensor, $\boldsymbol{\lambda}_1$, $\boldsymbol{\lambda}_2$ and $\boldsymbol{\lambda}_3$. These universal aspects include the preferential alignment of the vorticity vector with the intermediate eigenvector of the rate of strain tensor $\boldsymbol{\lambda}_2$ and the teardrop shape of the joint p.d.f. of the velocity gradient tensor invariants Q and R. In this study, three different turbulent flows have been considered: a TBL, a turbulent channel flow and homogenous isotropic turbulence. The resulting average pattern is very similar for all flow cases (figures 4–6) revealing a shear layer at 45° with the most stretching and compressing eigendirections, $\boldsymbol{\lambda}_1$ and $\boldsymbol{\lambda}_3$, which separates two larger-scale relatively uniform flow regions of opposing velocity directions. Vorticity associated with this shear layer is oriented in the direction of $\boldsymbol{\lambda}_2$ and is being stretched, which is expected since the eigenvalue associated with the intermediate eigenvector is positive on average. Furthermore, the shear layer contains stable foci, or vortices, aligned in the direction of the shear layer, which are separated by unstable node-saddle topologies.

The average pattern in the strain rate eigenframe contains an important asymmetric component in the form of the mentioned shear layer, which is also apparent in the average flow patterns around the vorticity vector and the swirling axis (figure 10). The statistical dominance of shear layers, together with the geometric relations between shear layers and the eigenvectors (see Jimenez 1992, §§ 2–3), explains the observed preferential alignment of the vorticity vector with the intermediate eigenvector in turbulence.

Furthermore, the average patterns offer an explanation for the teardrop shape of the joint p.d.f. of Q and R, suggesting this single point statistic has meaning in terms of an extended flow structure. In particular, the stable foci and the unstable node-saddle topologies within the shear layer, respectively, contribute to the tail along the right branch of the null-discriminant curve and the head skewed to the upper left in the QR joint p.d.f. The resulting joint p.d.f. for the average pattern is reminiscent of the teardrop for an actual instantaneous turbulent flow field.

Patterns similar to the average in the strain rate eigenframe are also frequently observed in the instantaneous realizations of the turbulent flows considered. It is therefore not an artifact of the employed averaging. This suggests that larger-scale uniform flow regions separated by shear layers containing several aligned vortices are a universal feature of turbulence, which is strongly linked to the other universal aspects of small-scale motion, i.e. vorticity alignment and QR joint p.d.f. Moreover, such an organization is characteristic for real turbulence and is not observed in random velocity fields.

The Australian Research Council and the Dutch Stichting FOM are gratefully acknowledged for their financial support. The authors would like to thank Professor Roger Fosdick and the reviewers for their helpful comments.

REFERENCES

Adrian, R. J., Meinhart, C. D. & Tomkins. C. D 2000 Vortex organization in the outer region of the turbulent boundary layer. *J. Fluid Mech.* **422**, 1–54.

Adrian, R. J. & Liu, Z. C. 2002 Observation of vortex packets in direct numerical simulation of fully turbulent channel flow. *J. Vis.* **5**, 9–19.

del Alamo, J. C., Jimenez, J., Zandonade, P. & Moser, R. D. 2004 Scaling of energy spectra of turbulent channels. *J. Fluid Mech.* **500**, 135–144.

del Alamo, J. C., Jimenez, J., Zandonade, P. & Moser, R. D. 2006 Self-similar vortex clusters in the turbulent logarithmic region. *J. Fluid Mech.* **561**, 329–358.

Andreotti, B. 1997 Studying Burgers' models to investigate the physical meaning of the alignments statistically observed in turbulence. *Phys. Fluids* **9**, 735–742.

Ashurst, W. T., Kerstein, A. R., Kerr, R. M. & Gibson, C. H. 1987 Alignment of vorticity and scalar gradient with strain rate in simulated Navier–Stokes turbulence. *Phys. Fluids* **30**, 2343–2353.

Batchelor, G. K. & Townsend, A. A. 1949 The nature of turbulent motion at large wave-numbers. *Proc. R. Soc. Lond.* A **199**, 238–255.

Betchov, R. 1956 An inequality concerning the production of vorticity in isotropic turbulence. *J. Fluid Mech.* **1**, 497–504.

Biferale, L., Chevillard, L., Meneveau, C. & Toschi, F. 2007 Multiscale model of gradient evolution in turbulent flows. *Phys. Rev. Lett.* **98**, 214501.

Blackburn, H. M., Mansour, N. N. & Cantwell, B. J. 1996 Topology of fine-scale motions in turbulent channel flow. *J. Fluid Mech.* **310**, 269–292.

Brandt, L., Schlatter, P. & Henningson, D. S. 2004 Transition in boundary layers subject to free-stream turbulence. *J. Fluid Mech.* **517**, 167–198.

Cantwell, B. J. 1992 Exact solution of a restricted Euler equation for the velocity gradient tensor. *Phys. Fluids* **4**, 782–793.

Cantwell, B. J. 1993 On the behavior of velocity gradient tensor invariants in direct numerical simulation of turbulence. *Phys. Fluids* **5**, 2008–2013.

Chacin, J. M. & Cantwell, B. J. 2000 Dynamics of a low Reynolds number turbulent boundary layer. *J. Fluid Mech.* **404**, 87–115.

Chong, M. S., Perry, A. E. & Cantwell, B. J. 1990 A general classification of three-dimensional flow fields. *Phys. Fluids* A **2**, 765–777.

Chong, M. S., Soria, J., Perry, A. E., Chacin, J., Cantwell, B. J. & Na, Y. 1998 A study of the turbulence structures of wall-bounded shear flows using DNS data. *J. Fluid Mech.* **357**, 225–248.

Elsinga, G. E., Adrian, R. J., van Oudheusden, B. W. & Scarano, F. 2010 Three-dimensional vortex organization in a high Reynolds number supersonic turbulent boundary layer. *J. Fluid Mech.* **644**, 35–60.

Elsinga, G. E., Kuik, D. J., van Oudheusden, B. W. & Scarano, F. 2007 Investigation of the three-dimensional coherent structures in a turbulent boundary layer. In *Forty-fifth AIAA Aerospace Sciences Meeting, Reno, NV. AIAA Paper* 2007-1305.

Elsinga, G. E. & Marusic, I. 2010 Evolution and lifetimes of flow topology in a turbulent boundary layer. *Phys. Fluids* **22**, 015102.

Elsinga, G. E., Scarano, F., Wieneke, B. & Van Oudheusden, B. W. 2006 Tomographic particle image velocimetry. *Exp. Fluids* **41**, 933–947.

Ganapathisubramani, B., Lakshminarasimhan, K. & Clemens, N. T. 2008 Investigation of three-dimensional structure of fine scales in a turbulent jet by using cinematographic stereoscopic particle image velocimetry. *J. Fluid Mech.* **598**, 141–175.

Ganapathisubramani, B., Longmire, E. K. & Marusic, I. 2003 Characteristics of vortex packets in the turbulent boundary layer. *J. Fluid Mech.* **478**, 35–46.

Gere, J. M. & Timoshenko, S. P. 1991 *Mechanics of Materials*, 3rd SI edn. Chapman and Hall.

Goto, S. 2008 A physical mechanism of the energy cascade in homogeneous isotropic turbulence. *J. Fluid Mech.* **605**, 355–366.

Guala, M., Lüthi, B., Liberzon, A., Tsinober, A. & Kinzelbach, W. 2005 On the evolution of material lines and vorticity in homogenous turbulence. *J. Fluid Mech.* **533**, 339–359.

Horiuti, K. & Fujisawa, T. 2008 The multi-mode stretched spiral vortex in homogeneous isotropic turbulence. *J. Fluid Mech.* **595**, 341–366.

Huang, M.-J. 1996 Correlations of vorticity and material line elements with strain in decaying turbulence. *Phys. Fluids* **8**, 2203–2214.

Hutchins, N. & Marusic, I. 2007 Evidence of very long meandering features in the logarithmic region of turbulent boundary layers. *J. Fluid Mech.* **579**, 1–28.

Jimenez, J. 1992 Kinematic alignment effects in turbulent flows. *Phys. Fluids* **4**, 652–654.

Jimenez, J., Wray, A. A., Saffman, P. G. & Rogallo, R. S. 1993 The structure of intense vorticity in homogeneous isotropic turbulence. *J. Fluid Mech.* **255**, 65–90.

Kerr, R. M. 1985 Higher-order derivative conclusions and the alignment of small-scale structures in isotropic numerical turbulence. *J. Fluid Mech.* **153**, 31–58.

Kevlahan, N. K. R. & Hunt, J. C. R. 1997 Nonlinear interactions in turbulence with strong irrotational straining. *J. Fluid Mech.* **337**, 333–364.

Kholmyansky, M., Tsinober, A. & Yorish, S. 2001 Velocity derivatives in the atmospheric turbulent flow at $Re_\lambda = 10^4$. *Phys. Fluids* **13**, 311–314.

Kida, S. & Tanaka, M. 1994 Dynamics of vortical structures in a homogeneous shear flow. *J. Fluid Mech.* **274**, 43–68.

Lüthi, B., Tsinober, A. & Kinzelbach, W. 2005 Lagrangian measurements of vorticity dynamics in turbulent flow. *J. Fluid Mech.* **528**, 87–118.

Meinhart, C. D. & Adrian, R. J. 1995 On the existence of uniform momentum zones in a turbulent boundary layer. *Phys. Fluids* **7**, 694–696.

Misra, A. & Pullin, D. I. 1997 A vortex-based subgrid stress model for large-eddy simulation. *Phys. Fluids* **9**, 2443–2454.

Moisy, F. & Jimenez, J. 2004 Geometry and clustering of intense structures in isotropic turbulence. *J. Fluid Mech.* **513**, 111–133.

Monty, J. P., Stewart, J. A., Williams, R. C. & Chong, M. S. 2007 Large-scale features in turbulent pipe and channel flows. *J. Fluid Mech.* **589**, 147–156.

Ohkitani, K. 2002 Numerical study of comparison of vorticity and passive vectors in turbulence and inviscid flows. *Phys. Rev.* E **65**, 046304.

Ooi, A., Martin, J., Soria, J. & Chong, M. S. 1999 A study of the evolution and characteristics of the invariants of the velocity-gradient tensor in isotropic turbulence. *J. Fluid Mech.* **381**, 141–174.

Passot, T., Politano, H., Sulem, P. L., Angilella, J. R. & Meneguzzi, M. 1995 Instability of strained vortex layers and vortex tube formation in homogeneous turbulence. *J. Fluid Mech.* **282**, 313–338.

Ringuette, M. J., Wu, M. & Martin, M. P. 2008 Coherent structures in direct numerical simulation of turbulent boundary layers at Mach 3. *J. Fluid Mech.* **594**, 59–69.

Rogallo, R. S. 1981 Numerical experiments in homogenous turbulence. *Tech. Rep.* TM 81315. NASA.

Ruetsch, G. R. & Maxey, M. R. 1991 Small-scale features of vorticity and passive scalar fields in homogeneous isotropic turbulence. *Phys. Fluids* A **3**, 1587–1597.

Ruetsch, G. R. & Maxey, M. R. 1992 The evolution of small-scale structures in homogeneous isotropic turbulence. *Phys. Fluids* A **4**, 2747–2760.

Schröder, A., Geisler, R., Staack, K., Wieneke, B., Elsinga, G. E., Scarano, F., Henning, A. 2008 Lagrangian and Eulerian views into a turbulent boundary layer flow using time-resolved tomographic-PIV. *14th Intl. Symp. on Applications of Laser Techniques to Fluid Mechanics, Lisbon, Portugal. Exp. Fluids* (submitted, 2009).

She, Z.-S., Jackson, E. & Orszag, S. A. 1990 Intermittent vortex structures in homogeneous isotropic turbulence. *Nature* **344**, 226–228.

Soria, J., Sondergaard, R., Cantwell, B. J., Chong, M. S. & Perry, A. E. 1994 A study of the fine-scale motions of incompressible time-developing mixing layers. *Phys. Fluids* **6**, 871–884.

Swearingen, J. D. & Blackwelder, R. F. 1987 The growth and breakdown of streamwise vortices in the presence of a wall. *J. Fluid Mech.* **182**, 255–290.

Tomkins, C. D. & Adrian, R. J. 2003 Spanwise structure and scale growth in a turbulent boundary layers. *J. Fluid Mech.* **490**, 37–74.

Tsinober, A. 2001 *An Informal Introduction to Turbulence*. Kluwer.

Tsinober, A., Kit, E. & Dracos, T. 1992 Experimental investigation of the field of velocity gradients in turbulent flows. *J. Fluid Mech.* **242**, 169–192.

Vieillefosse, P. 1984 Internal motion of a small element of fluid in an inviscid flow. *Physica* A **125**, 150–162.

Vincent, A. & Meneguzzi, M. 1994 The dynamics of vorticity tubes in homogeneous turbulence. *J. Fluid Mech.* **258**, 245–254.

Westerweel, J., Fukushima, C., Pedersen, J. M. & Hunt, J. C. R. 2009 Momentum and scalar transport at the turbulent/non-turbulent interface of a jet. *J. Fluid Mech.* **631**, 199–230.

Zhou, J., Adrian, R. J., Balachandar, S. & Kendall, T. M. 1999 Mechanisms for generating coherent packets of hairpin vortices in channel flow. *J. Fluid Mech.* **387**, 353–396.